Mineralogy and Petrology (2005) 84: 169–187
DOI 10.1007/s00710-005-0079-3

Mineralogy and Petrology
Printed in Austria

Chromitites of komatiitic affinity from the Archaean Nuggihalli greenstone belt in South India

M. Bidyananda[1] and **S. Mitra**[2]

[1] Wadia Institute of Himalayan Geology, Dehra Dun, India
[2] Department of Geological Sciences, Jadavpur University, Kolkata, India

Received September 6, 2004; revised version accepted March 2, 2005
Published online April 30, 2005;
Editorial handling: J. G. Raith

Summary

Mineral chemistry and petrological data of chromites from chromitite bands in the N–S trending schist belt of Nuggihalli (southern Karnataka, India), belonging to the Dharwar craton of South India, are presented in this paper. Crystal chemical data indicate a komatiitic affinity of the chromitite. *P–T* calculations of the chromite-hosting peridotites yielded a pressure range of 13 to 28 kbar and temperatures ranging from 775 to 1080 °C; the oxygen fugacity ($\log fO_2$) varies from +0.5 to +1.6 above the QFM buffer. The *P*, *T* and fO_2 data indicate that Nuggihalli chromitites crystallized in an environment akin to the upper mantle. The studied samples also show partial resetting; the lower temperatures ranging from 515 to 680 °C are ascribed to subsequent metamorphism of the area.

Introduction

Spinels crystallizing in the early cooling history of basic magma are chromium-rich, because Cr^{3+} stronger partitions in the octahedral site of spinel structure than in the melt. The Cr^{3+} ion manifests strong crystal field stabilization energy at the octahedral site (*cf.*, 224 kJ/mol, *Mitra*, 1996, page 73, Table 3.2.1), which is higher than for other transition elements. Thus, Cr^{3+} is enriched in spinels crystallizing early from a basic magma, which form mostly as a product of partial melting of peridotitic mantle. Spinel compositions reflect a complex function of magma (and source peridotite) composition, crystallization temperature and cooling rate. Thus, in conjunction with co-liquidus olivine in primitive magmas, chromite (chromian-spinel) composition offers the potential for deciphering the petrogenetic aspects of such magmas, including information about the source of the peridotite. A large

database exists in the literature reporting on the chromite deposits from different tectonic settings but only a few occurrences of chromitite in komatiites are reported, e.g., from Belingwe, Zimbabwe (*Zhou* and *Kerrich*, 1992), Kuhmo, Finland (*Liipo* et al., 1995), Inyala, Southern Zimbabwe (*Rollinson*, 1997) and Western Australia (*Barnes*, 1998, 2000).

In the present study, mineral chemical data of the chromites from the chromitites and associated silicate and oxide phases from the chromite-bearing peridotite are reported for further enhancement of the knowledge about chromitite occurring in association with the komatiite affinity Archean (>3.1 Ga, *Bidyananda* et al., 2003) Nuggihalli greenstone belt of South India. We have previously studied some of the chromitite samples by combined electron microprobe analysis, single crystal X-ray measurements, low temperature (77 K) (*Lenaz* et al., 2004) as well as room temperature (298 K) Mössbauer spectroscopy (*Bidyananda* and *Mitra*, 2004). In the present study, we also refer to these earlier reported data and use them to decipher the crystallization conditions of the studied samples.

Geological setting

The Nuggihalli schist belt forms a roughly NW–SE to N–S striking belt of low to medium grade rocks in the Dharwar craton (Fig. 1). It belongs to the greenstone belts in South India. Ultramafic rocks in this belt include chromite-bearing serpentinised peridotite and talc-chlorite-tremolite schists. Other major rock types are amphibolites, metasediments (fuchsite quartzite, quartz-mica-chlorite schist and staurolite-quartz-mica schist), tonalitic-trondhjemitic gneisses and meta-anorthosite. Algoma-type (banded iron formation) titanomagnetite bodies rich in vanadium are intercalated with the ultramafic rocks. The study area has been subjected to greenschist to amphibolite facies metamorphism and increases in grade from north to south (*Ramakrishnan*, 1981). So far the metamorphic age of the area is not ascertained. Based on the presence of pillow and spinifex textures in peridotites from adjacent areas, *Naqvi* and *Hussain* (1979) reported these rocks as submarine extrusive metavolcanics. *Sudhakar* (1980) pointed out the komatiitic affinity of these serpentinites mainly on the basis of their Cr/Al ratios. After establishing the komatiitic affinity of the ultramafic rocks within this belt, it was compared to Archaean greenstone belts such as those in the Barberton area.

In the study area, the ultramafic rocks are exposed as discontinuous lenticular bodies. At the western margin of the belt, the ultrabasic rocks have undergone intense shearing. Chromitite bodies are confined to the basal portion of the serpentinised peridotite. Completely serpentinised rocks preserved pillow textures in the Tagadur and Bhaktarhalli areas (Fig. 1). So far there is no conclusive evidence regarding the nature of these ultrabasic rocks and age data are lacking. But they are older than the surrounding gneisses (>3.1 Ga, *Bidyananda* et al., 2003) and have been affected by subsequent metamorphic events. The chromitite seams occur commonly as layers, high angle bands and irregular tabular or lensoid bodies within serpentinite (*Bidyananda*, 2000). Several abandoned mines are present throughout the belt. Currently mined chromite deposits are located at Byrapur, Bhaktarhalli, Tagadur and Jambur areas (Fig. 1). The variable shape and size of the ore bodies appear to be controlled by their position in the limbs and hinges of early and late

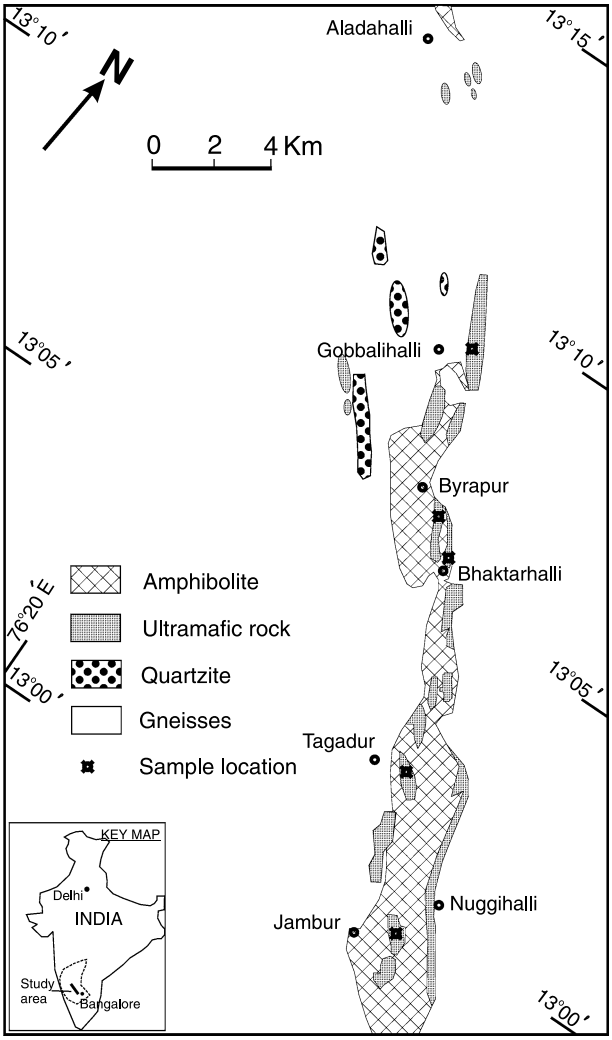

Fig. 1. Geological map of the Nuggihalli schist belt showing sample locations (modified from *Jafri* et al., 1983)

stage folds and dislocation of the ore bodies due to shearing. The shape and size of the chromite deposits varies from lenticular (∼300 m long × 6 m wide) at the Tagadur mines to podiform (>60 m long, 6 m wide and extending to a depth of ∼150 m) in the Byrapur underground mine. Lenticular deposits occur at Bhaktarhalli, Aladahalli and Gobbalihalli areas as well.

Analytical techniques

Chromites from sieved samples (60 to 80 mesh size) were separated by hand picking for X-ray diffractometry (XRD) and Mössbauer analyses. The separated samples were pulverized to about 100 mesh and then cleaned in running water. The remaining silicate minerals were picked up and the spinel samples were repeatedly passed through a Frantz isodynamic magnetic separator. The samples were then treated with warm dilute HCl and the silicates were further separated in clerici solution and washed. After separation the samples were finely pulverized (∼350

mesh) in agate mortar till homogeneity of grain size was ensured. For the mineral chemical study, the chromian-spinel samples were polished by Buehler Automat (model no. 850) and other polishing auxiliaries and were analysed by a JEOL-733 Superprobe micro-analyser with wave-length dispersive method at 15 kV, with a beam current of 0.01 μA, beam diameter of 10 μm and counting times of 50 seconds. Samples were calibrated with reference to natural mineral standards and data were reduced by *Bence* and *Albee* method (1968).

Petrography

Peridotite

Primary silicate phases of the ultramafic rocks associated with the studied chromite have been altered to serpentinite and chlorite. However, unaltered relicts of

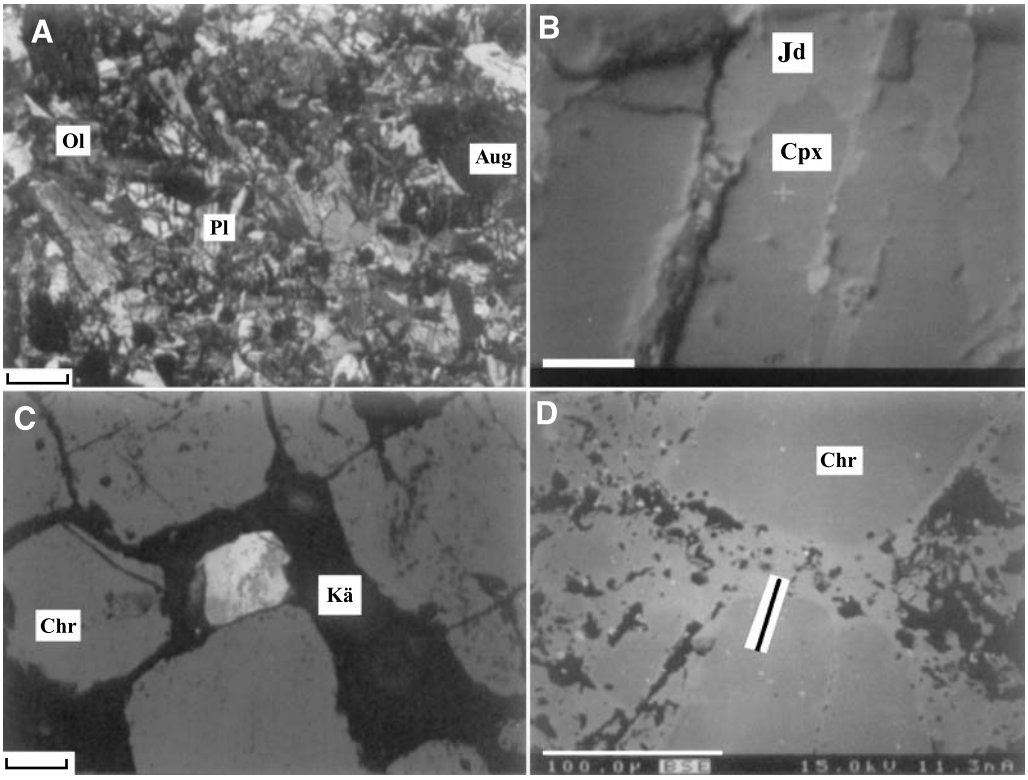

Fig. 2. **A** Photomicrograph of peridotite showing medium-grained, holocrystalline texture; olivine (Ol) crystals in association with plagioclase (Pl) enclose the subhedral clinopyroxene (augite, Aug). Scale 1 cm = 0.017 mm. **B** BSE image of clinopyroxene (Cpx) and jadeite (Jd) intergrowth in peridotite. Darker shaded Cpx (augite) is replaced by lighter shaded jadeite. Aluminous chromite occurs as white patches in clinopyroxene. **C** Photomicrograph showing euhedral grains of chromite (Chr) cemented by chromian chlorite (kämmererite, Kä) gangue. Light color (patchy) euhedral grain at the center is nickel oxide (NiO = 97.80%). Scale: 1 cm = 0.017 mm. **D** BSE image of fragmented chromite (Chr) grains showing ferrian chromite rims with higher magnification

olivine and pyroxene as cumulus phases are sporadically present. Photomicrographs and backscattered electron images of this rock containing unaltered relict phases are presented in Figs. 2A and B, respectively. Serpentinite is fibrous in nature and occurs radially around the unaltered relicts of pyroxene and olivine. Dolomite and magnesite are present in veins in the serpentinites and talc occurs as fracture fillings.

Chromitite

Cumulus textures are a common primary magmatic feature of the studied chromitites. Chromite grains are commonly anhedral to subhedral occurring in a serpentine matrix. Low temperature hydrous minerals such as serpentine and chlorite and other phases like pyrite, pentlandite and disseminated nickel oxides (Fig. 2C) occur as inclusions within and in contact with chromite grains. Occasional occurrence of euhedral chromite moulding around serpentine and synneusis texture in which chromite crystals surround silicate phases in the form of a chain are observed. Oxidation rims, characterized by higher brightness in backscattered electron (BSE) images, are commonly developed around chromite grains and along fracture zones (Fig. 2D).

Mineral chemistry

Peridotite

The major mineralogical phases such as olivine, pyroxene, plagioclase, Cr-chlorite, serpentine and amphibole of the chromite-hosting serpentinised peridotite were analyzed. Representative analyses are given in Table 1. It may be noted that some analytical data fall short of the required total cations for the ideal stoichiometries. Deviation from the ideal mineral stoichiometry is generally explained with (i) lack in determination of Fe^{3+} and (ii) presence of vacancies in the crystal lattice.

Olivine

Olivine-bearing samples show extensive alteration to serpentine and/or chlorite. In most cases remnants of olivine occur as relicts in the serpentine matrix. Olivine grains do not show any strain effects (e.g., undulose extinction, deformation bands etc.) and individual grains are optically very homogenous. The chemical composition of olivine ranges from Fo_{83} to Fo_{92}; the Fo content varies amongst the grains. MnO contents of analyzed olivine ranges from 0.14 to 0.22 wt%, and CaO varies from 0.20 to 0.26 wt% (Table 1). Analyzed olivines are devoid of Cr_2O_3 and NiO. The *mg*-numbers (Mg/Mg + Fe) of olivine range between 0.86 and 0.90.

Pyroxene and amphibole

Clinopyroxene without exsolved orthopyroxene lamellae is present as intercumulus phase in the peridotites, whereas blebs of orthopyroxene occur as relict phase in the

Table 1. *Electron microprobe analyses of representative mineral phases of the chromite-bearing serpentinised peridotite*

Mineral phase	Olivine				Clinopyroxene				Jadeite	Actinolite		Plagioclase	
Anal. no.	1	2	3	4	1	2	3	4	5	1	2	1	2
SiO_2	40.42	41.06	40.64	40.47	53.25	51.73	50.77	50.65	58.05	52.53	53.49	51.55	51.05
TiO_2	0.00	0.00	0.00	0.00	0.19	0.19	0.20	0.31	0.02	0.17	0.15	0.04	0.05
Al_2O_3	0.09	0.01	0.05	0.10	2.98	2.74	3.41	3.59	20.21	4.37	3.96	28.74	29.20
Cr_2O_3	0.00	0.00	0.00	0.00	0.00	0.55	1.13	1.02	0.00	0.62	0.39	0.01	0.00
FeO*	12.03	10.16	12.48	13.17	6.76	8.20	6.62	6.72	1.21	8.51	8.12	1.13	0.85
MnO	0.22	0.17	0.17	0.14	0.10	0.19	0.15	0.19	0.01	0.12	0.16	0.04	0.00
MgO	46.53	48.60	46.03	45.16	20.19	19.85	18.54	18.44	1.47	18.42	18.68	0.23	0.19
NiO	–	–	–	–	0.00	0.05	0.09	0.00	0.00	0.04	0.00	0.00	0.00
Na_2O	0.01	0.00	0.02	0.00	0.17	0.21	0.25	0.25	14.32	1.29	1.03	4.09	3.77
K_2O	0.00	0.02	0.00	0.00	0.00	0.01	0.01	0.01	0.31	0.05	0.08	0.23	0.23
CaO	0.25	0.26	0.25	0.20	15.38	15.74	17.76	17.37	4.12	12.26	12.15	12.94	13.60
Total	99.55	100.28	99.64	99.24	99.01	99.46	98.93	98.55	99.72	98.38	98.21	99.00	98.94
Number of Oxygens													
	4	4	4	4	6	6	6	6	6	23	23	8	8
Si	1.005	1.004	1.011	1.013	1.942	1.906	1.881	1.882	2.001	7.417	7.524	2.353	2.373
Ti	0.000	0.000	0.000	0.000	0.005	0.002	0.005	0.009	0.001	0.018	0.016	0.002	0.001
Al	0.003	0.000	0.001	0.003	0.128	0.118	0.148	0.156	0.821	0.727	0.657	1.587	1.560
Cr	0.000	0.000	0.000	0.000	–	0.014	0.033	0.031	0.000	0.069	0.043	0.000	0.000
Fe*	0.250	0.208	0.260	0.276	0.206	0.252	0.204	0.210	0.033	1.005	0.955	0.033	0.043
Mn	0.005	0.004	0.004	0.003	0.003	0.004	0.004	0.007	0.000	0.014	0.019	0.000	0.002
Mg	1.725	1.772	1.707	1.686	1.098	1.089	1.022	1.020	0.076	3.877	3.917	0.013	0.016
Ni	0.000	0.000	0.000	0.000	–	0.001	0.002	–	0.000	0.005	0.000	0.000	0.000
Na	0.000	0.000	0.001	0.000	0.012	0.013	0.018	0.009	0.957	0.353	0.21	0.337	0.365
K	0.000	0.001	0.000	0.000	0.000	0.000	0.000	–	0.014	0.009	0.014	0.014	0.014
Ca	0.007	0.007	0.007	0.005	0.601	0.619	0.706	0.692	0.152	1.855	1.831	0.638	0.672
Total	2.994	2.996	2.989	2.986	3.995	4.018	4.023	4.016	4.055	15.349	15.176	5.010	5.013

(*continued*)

Table 1 (*continued*)

Mineral phase	Olivine				Clinopyroxene				Jadeite	Actinolite		Plagioclase	
Anal. no.	1	2	3	4	1	2	3	4	5	1	2	1	2
*mg***	0.87	0.90	0.87	0.86	0.84	0.81	0.83	0.83	0.70				
Wo %					31.60	31.58	36.54	36.00					
En					57.60	55.56	52.90	53.07					
Fs					10.80	12.86	10.56	10.93					

Cr-clinochlore					Bunsenite (NiO)	Serpentine		Calcite	Magnetite	
Sample	T7-1	T7-2	B1	B2		1	2			
SiO_2	28.95	28.73	28.81	29.03	0.00	50.31	43.95	0.11	0.37	0.22
TiO_2	–	–	0.12	0.05	0.00	0.01	0.00	0.00	17.04	15.58
Cr_2O_3	1.86	1.02	3.09	3.67	0.55	0.13	0.00	0.15	4.08	3.07
Al_2O_3	22.54	21.96	20.10	18.12	0.01	0.57	1.26	0.06	3.18	3.44
Fe_2O_3	–	–	–	–	–	–	–	–	27.44	31.11
FeO*	5.49	5.28	2.36	2.26	0.19	3.67	3.27	0.69	45.81	43.46
MnO	–	–	0.03	0.01	0.02	0.07	0.00	0.35	0.37	1.02
MgO	29.02	30.31	30.68	30.93	0.00	32.87	38.14	0.23	0.74	0.81
NiO	0.28	0.19	0.46	0.34	97.80	0.19	0.98	0.01	0.01	0.00
CaO	–	–	0.02	0.03	0.03	0.36	0.00	57.61	0.20	0.14
Na_2O	0.03	0.02	0.00	0.02	0.07	0.03	0.00	0.06	0.05	0.04
K_2O	–	–	0.01	0.02	0.00	0.05	0.00	0.01	–	0.02
Total	88.17	87.51	85.68	84.48	98.66	88.29	84.33	59.27	99.29	98.91
Number of Oxygens	28	28	28	28	10	7	7	6	32	32
Si	5.700	5.560	5.560	5.520	0.000	2.279	2.045	0.009	0.112	0.064
Al	4.380	5.060	4.820	4.430	0.000	0.033	0.069	0.006	1.112	1.208

(*continued*)

Table 1 (*continued*)

Cr-clinochlore					Bunsenite (NiO)	Serpentine		Calcite	Magnetite	
Sample	T7-1	T7-2	B1	B2		1	2			
Ti	0.020	0.020	0.000	0.000	0.000	–	–	–	3.808	3.496
Cr	0.280	0.160	0.460	0.560	0.061	0.005	–	0.012	0.960	0.720
Fe^{3+}	–	–	–	–	–	–	–	–	6.128	6.984
Fe^{2+}	0.860	0.840	0.380	0.360	0.023	0.139	0.129	0.054	11.376	10.832
Mn	–	–	0.000	0.000	0.002	0.003	–	0.027	0.096	0.256
Mg	8.140	8.600	8.830	9.040	0.000	2.218	2.664	0.033	0.328	0.360
Ni	0.060	0.040	0.000	0.070	9.879	0.008	0.036	–	0.000	0.000
Ca	–	–	0.000	0.000	0.000	0.016	–	5.844	0.064	0.048
Na	0.010	–	0.000	0.000	0.016	–	–	0.012	0.032	0.024
K	–	–	0.000	0.000	0.000	0.003	–	–	0.000	0.008

In EPMA analysis total iron was calculated as FeO. * FeO and Fe_2O_3 in magnetite are calculated based on the stoichiometry. ** $mg = Mg/(Mg + Fe)$

rock. Intergrowths of augite and jadeite were observed and confirmed by back-scattered electron imaging (Fig. 2B). Representative analyses of the two phases are presented in Table 1 (Analyses #3, 4 augite and #5 jadeite). In clinopyroxene CaO contents range between 15.38 and 17.76 wt%; such sub-calcic clinopyroxenes were rarely reported in peridotite. The low Ca contents of clinopyroxene indicate a high equilibrium temperature. Al_2O_3 varies from 2.74 to 3.59 wt% and the *mg*-numbers range from 0.81 to 0.84. The majority of the analyzed pyroxenes are chromian ($Cr_2O_3 = 0.00–1.13$ wt%), the samples are slightly titaniferous ($TiO_2 = 0.19–0.31$ wt%) and sodic ($Na_2O = 0.11–0.25$ wt%). The wollastonite component is low (Wo = 25.50–36.54%).

Actinolite is the most common amphibole in the metamorphosed peridotite. Representative analyses of actinolite, calculated on the basis of 23 oxygens, are presented in Table 1. Their *mg*-numbers range from 0.79 to 0.80, TiO_2 content varies from 0.15 to 0.17 wt% and amphiboles are slightly chromiferous ($Cr_2O_3 = 0.39–0.62$ wt%). K_2O is present in trace amounts.

Chromian chlorite

Chromian chlorite is commonly found in association with ferrian chromite. Representative analyses are shown in Table 1. Recalculation of cations based on 28 oxygens are close to the ideal chlorite formula, the sum of cations in the tetrahedral site being equal to 8 and that in the octahedral site totaling 12. MgO ranges from 30.68 to 30.93 wt% in chromiferous ($Cr_2O_3 = 1.86–3.67$) samples, chlorites with low Cr_2O_3 have lower MgO, ranging from 24.56–24.72 wt% (*Mitra* and *Bidyananda*, 2001). Following *Bailey* et al.'s (1979) nomenclature the chlorite is classified as clinochlore. Per formula unit contents of different cations (28 O basis) are: Si (5.52–5.70), Cr (0.160 to 0.560), ^{IV}Al (2.300–2.540) and ^{VI}Al (1.900–2.520). Chlorite grains adjacent to the chromite are more enriched in Cr than those farther away.

Serpentine

Serpentine minerals showing platy as well as fibrous habit are commonly observed in the studied samples. They occur as inclusions within or surrounding the chromite. Serpentine has some compositional variation; one analysis has much higher SiO_2 and lower MgO (Table 1, #1). The Al_2O_3 content is low (0.57–1.26 wt%). Total FeO varies between 3.27–3.67 wt%, NiO ranges between 0.19–0.98 wt%. Representative EPMA analyses of plagioclase, Ti-bearing magnetite and nickel oxide (bunsenite) are also presented in Table 1. Nickel oxide (NiO = 97.80 wt% without sulphur) occurs as an isolated grain in the Cr-chlorite matrix and surrounded by chromite (Fig. 2C).

Chemical composition of chromite

Chromite occurring as cumulus phase in the ultramafic rocks is by far the most dominant phase. Representative chemical analyses of the studied chromites are presented in Table 2. The analyzed oxides were recalculated on the basis of 32 oxygens.

Table 2. *Representative electron probe microanalyses of chromites from the Nuggihalli schist belt*

Sample	Gob-7a	Gob-7c	By-5	By[2]	BRG[2]	By[†]	T[†]	J[†]	G-1	J-6a	J-6b
SiO_2	0.10	0.04	0.03	0.03	0.06	0.03	0.18	0.08	0.23	0.03	0.04
TiO_2	0.15	0.13	0.18	0.53	0.28	0.48	0.29	0.13	0.13	0.54	0.64
Cr_2O_3	51.38	54.84	55.70	57.73	56.57	57.98	49.92	44.54	39.51	54.31	54.37
Al_2O_3	14.41	12.14	9.03	6.39	9.56	6.51	10.04	17.92	21.59	6.73	3.60
Fe_2O_3	2.55	2.25	4.30	5.91	3.60	19.62	21.31	24.88	4.74	7.68	10.51
FeO	22.76	23.09	26.62	19.54	19.85	5.78	7.09	8.04	27.95	27.80	27.98
MnO	0.69	0.69	0.76	0.41	0.44	0.42	0.72	0.65	0.59	0.47	0.50
MgO	7.08	6.75	4.28	8.70	8.67	9.10	10.42	3.67	4.44	3.66	3.04
NiO	0.33	0.04	0.10	0.00	0.00	0.05	0.02	0.10	0.00	0.04	0.05
CaO	0.02	0.00	0.00	0.00	0.00	0.00	0.00	0.00	0.00	0.00	0.00
Na_2O	0.00	0.00	0.00	0.00	0.00	0.00	0.02	0.00	0.04	0.02	0.04
K_2O	0.00	0.00	0.00	0.00	0.00	0.00	0.00	0.04	0.03	0.00	0.02
Total	99.18	99.97	101.00	99.26	99.03	99.98	100.01	100.05	99.26	101.24	100.74
Cations based on 32 Oxygens											
Si	0.024	0.008	0.008	0.008	0.016	0.007	0.046	0.023	0.064	0.008	0.008
Ti	0.032	0.024	0.040	0.112	0.056	0.095	0.054	0.023	0.024	0.112	0.136
Cr	10.840	11.632	12.096	12.528	12.088	12.020	10.189	8.862	8.224	11.952	12.264
Al	4.536	3.840	2.928	2.056	3.048	2.019	2.679	5.278	6.696	2.208	1.208
Fe^{3+}	0.512	0.456	0.888	1.200	0.736	3.881	3.737	4.764	0.936	1.608	2.256
Fe^{2+}	5.080	5.184	6.120	4.424	4.464	1.260	2.520	1.712	6.152	6.472	6.680
Mn	0.152	0.160	0.176	0.096	0.104	0.095	0.155	0.137	0.128	0.112	0.120
Mg	2.816	2.704	1.752	3.568	3.408	3.563	3.998	1.391	1.744	1.520	1.296
Ni	0.086	0.007	0.022	0.000	0.000	0.009	0.005	0.015	0.000	0.009	0.010
Ca	0.008	0.000	0.000	0.000	0.000	0.000	0.000	0.000	0.000	0.000	0.000
Na	0.000	0.000	0.000	0.000	0.000	0.006	0.003	0.000	0.024	0.008	0.024
K	0.000	0.000	0.000	0.000	0.000	0.000	0.000	0.006	0.008	0.000	0.008
Fe^{3+}/Fe^{2+}	0.101	0.088	0.145	0.271	0.165	3.080	1.483	2.783	0.152	0.248	0.338

* Total Fe was calculated from EPMA counts as FeO, which was recalculated to FeO and Fe_2O_3 based on (a) the distribution in a normal spinel [†] (b) room temperature Mössbauer study [2] (c) by single crystal X-ray and low temperature Mössbauer study

Total iron was recalculated to Fe^{2+} and Fe^{3+} accordingly. Cr_2O_3 content varies between 39 and 58 wt%. Based on the Cr_2O_3 concentrations, the studied samples can be broadly grouped into two categories (I) Cr_2O_3 >50 wt% (II) Cr_2O_3 <50 wt%. The cluster with higher Cr_2O_3 content may reflect a higher degree of partial melting of a peridotitic source rock (*Dick* and *Bullen*, 1984). The first group represents tabular, dyke-like and layered chromitite deposits, the second group forms relatively small lensoid deposits. In type I Al_2O_3 varies from 3.60 to 14.41 whereas in type II Al_2O_3 values range from 10.04 to 21.59. TiO_2 contents range from 0.13 to 0.64 wt% but such a compositional range is observed within any chromite deposit. TiO_2 does not show a correlation with any other major element in the studied chromite samples.

In some of the samples, chromite crystals are characterized by brighter rims in reflected light and BSE images (Fig. 2D). Systematic microprobe analyses along traverses (rim to core) within single grains from two samples were carried out. The

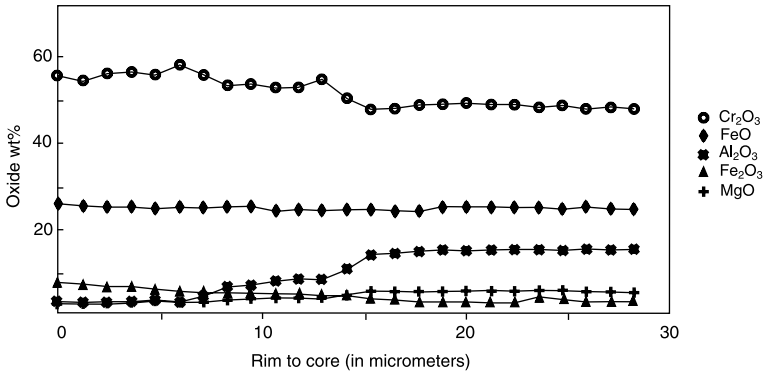

Fig. 3. Compositional variation from rim to core in a ferrain chromite. BSE image of the analyzed grain is presented in Fig. 2D

results show an increase in Cr, Fe^{3+}, and Fe^{2+} and a decrease in Mg, and Al in the higher reflectant zones (Fig. 2D). About 15 μm away from rim (Fig. 3) we see a distinct change in the concentration of Al_2O_3, which increases at the expense of Cr_2O_3; while the FeO and Fe_2O_3 concentrations remain constant.

Graphical presentation of chromite composition

To establish the nature of the studied chromitites from the Archaean greenstone belts of South India various compositional diagrams were used. The studied samples plot in the aluminian and ferrian chromite field in *Steven*'s (1944) triangular diagram (not shown). Chromite compositions were also plotted in the $100 \times Cr/(Cr + Al)$ vs. $100 \times Mg/(Mg + Fe^{2+})$ diagram (not shown). In this diagram the data cluster along with the well-known stratiform deposits of the world (e.g., Bushveld, Muskox, Stillwater etc.). In the modified $Fe^{3+} \times 100/(Cr + Al + Fe^{3+})$ vs. $Mg \times 100/(Mg + Fe^{2+})$ diagram (Fig. 4) the chromite analyses plot in the combined stratiform and komatiitic field. However, it must be emphasized that this plot does not

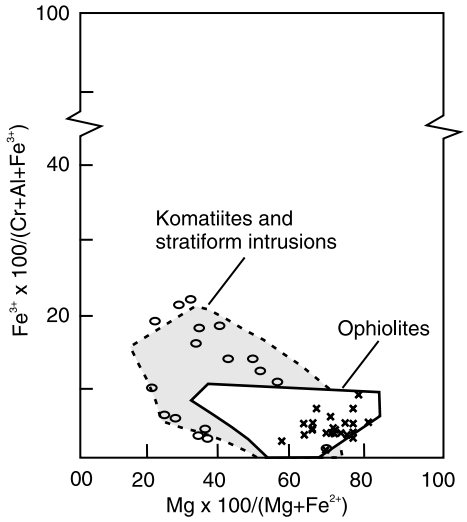

Fig. 4. Composition of chromite (○) plotted on projections of *Steven*'s (1944) spinel prism. The field for the various types of complexes shown are based on *Irvine* (1967), *Bird* and *Clark* (1976) and *Zhou* and *Kerrich* (1992). Ophiolitic chromite (×) data are from *Melcher* et al. (1997) and *Proenza* et al. (1999, 2004)

allow to differentiate chromite from komatiites and stratiform deposits; all plot in the same compositional field (*Mitra* and *Bidyananda*, 2003). In the Cr_2O_3 vs. Al_2O_3 wt% plot (Fig. 5) the studied samples clearly show komatiitic affinity. We have used the $Cr/Cr + Al$ vs. $Fe^{2+}/Fe^{2+} + Mg$ plot (*Rollinson*, 1997; Fig. 6) to compare the studied chromitites with reported komatiitic chromitite of Zimbabwe (Belingwe, Inyala and Shurugwi). As these komatiites are very well studied and the freshest ones among the Archaean komatiites, they are suitable for correlation in deciphering the primary magmatic nature. The $Cr/Cr + Al$ values of our samples and the Zimbabwe dataset approximately fall in the same range (0.60 to 0.90) while the $Fe^{2+}/Fe^{2+} + Mg$ ratios of the Nuggihalli samples show wider variation

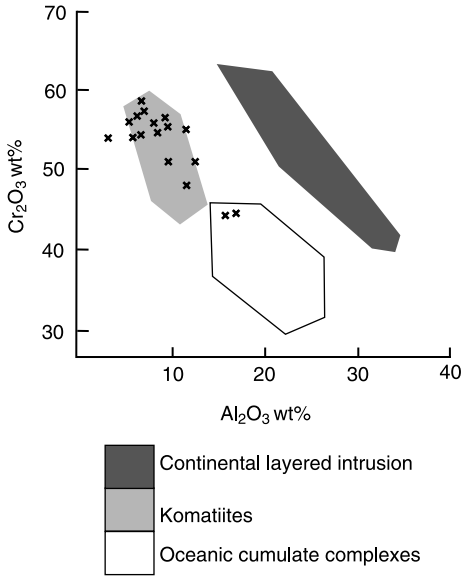

Fig. 5. Discrimination diagrams for chromite composition plotted in terms of Cr_2O_3 vs. Al_2O_3. Modified from a four-component diagram of *Bai* and *Zhou* (1988)

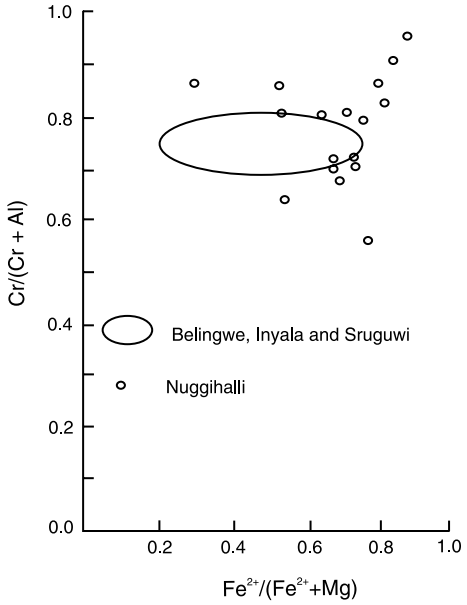

Fig. 6. $Cr/(Cr + Al)$ vs. $Fe^{2+}/(Fe^{2+} + Mg)$ plot (*Rollinson*, 1997) of the studied Cr-spinels in comparison with chromitites from komatiites of Belingwe, Inyala and Shruguwi greenstone belts, Zimbabwe

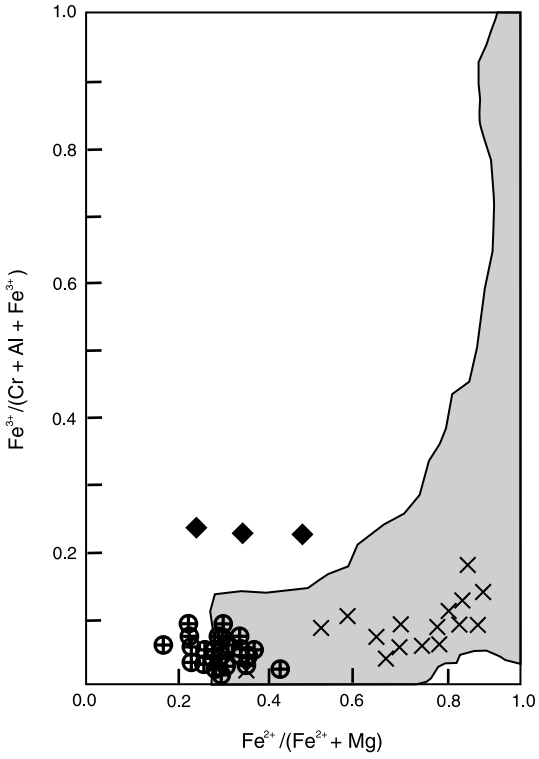

Fig. 7. Nuggihalli chromite (×) plotted on $Fe^{3+}/(Cr + Al + Fe^{3+})$ vs. $Fe^{2+}/(Fe^{2+} + Mg)$ diagram of *Barnes* and *Roeder* (2001), shaded portion komatiite zone, ◆ (black diamond) represent the three samples for which Fe^{3+} was determined by room temperature Mössbauer analysis. Phanerozoic massive chromitites (⊕) are also plotted for comparison, data are from *Melcher* et al. (1997) and *Proenza* et al. (1999, 2004)

than the Zimbabwe chromites. We have also plotted our chromite data in the $Fe^{3+}/(Cr + Al + Fe^{3+})$ vs. $Fe^{2+}/(Fe^{2+} + Mg)$ diagram (*Barnes* and *Roeder*, 2001; Fig. 7) and the studied chromitite is compared with the massive Phanerozoic chromitites. All the studied samples (except By†, T† and J†; Table 2) show clear komatiitic affinity, whereas the Phanerozoic chromitites fall on the margin of the compositional field. The anomalous nature of the three data (black diamonds, in Fig. 7) may arise from the contribution of oxidized rim material mixed in the powder samples for room temperature Mössbauer studies, leading to a higher Fe^{3+} content. In contrast, two unaltered samples (By and BRG; Table 2) studied by combined XRD, low temperature Mössbauer spectroscopy and EPMA show distinct komatiitic nature (Fig. 7).

Chromite equilibration conditions

Chromite being physicochemically a very stable phase, is an useful indicator of the crystallization conditions of chromite-bearing rocks (e.g., *Irvine*, 1967; *Hill* and *Roeder*, 1974; *Dick* and *Bullen*, 1984). In the following, we present the results of temperature, pressure and oxygen fugacity calculations on the chromitites in order to establish their crystallization conditions.

Equilibration temperature

Mg–Fe partitioning relations among oxide phases like spinel and ferromagnesian silicate phases viz. olivine, is the most commonly used type of geothermometer to

Table 3. *Equilibrium temperature of the study area in comparison with the reported temperatures from greenstone belts of Zimbabwe by different workers*

Temperature (°C)	Area	Reference
1100–1200	Belingwe	*Zhou* and *Kerrich* (1992)
1100–1200	Inyala	*Rollinson* (1997)
515–775	Nuggihalli	Present work (using *Ballhaus* et al., 1991)
920–1080	Nuggihalli	Present work (using *Princivalle* et al., 1999)

determine the equilibrium temperature in mantle rocks (*Irvine*, 1965; *Evans* and *Frost*, 1975; *Fabries*, 1979; *Roeder* et al., 1979; *Sack* and *Ghiorso*, 1991; *O'Neill* and *Wall*, 1987; *Ballhaus* et al., 1991). Extensive cation exchange and resetting of temperatures may occur during cooling, but only if the cooling rate is low enough, and thus a long time is available for diffusion to proceed. The chromite-olivine geothermometer may, therefore, have application as a 'cooling speedometer'. Using the *Fabries* (1979) calibration, we previously reported temperatures of 1178 °C for the Nuggihalli samples (*Mitra* and *Bidyananda*, 2003). Actual recalculation of the equilibrium temperatures of the studied samples using *Ballhaus* et al.'s (1991) formulation revealed much lower temperatures ranging from 515 to 680 °C (Table 3). The low temperatures likely represent sub-solidus re-equilibration related to the later metamorphic overprint. A single temperature (775 °C) equivalent to the lower limit of the *Barnes*'s (2000) komatiitic chromite relict igneous equilibrium temperature was calculated from an olivine-chromite pair.

Many workers have investigated the dependence of the cation distribution on temperature (*O'Neill* and *Navrotsky*, 1983, 1984; *Della Giusta* and *Ottonello*, 1993; *Nell* and *Wood*, 1991). We also used the structural refinement data determined from single crystal X-ray study (*Lenaz* et al., 2004) to calculate the equilibrium temperature in the studied samples. *Della Giusta* et al. (1996), based on the study of Mg–Al spinel, proposed the following geothermometer,

$$T(^{\circ}\mathrm{C}) = \mathrm{C1} - \mathrm{C2}\times\mathrm{B} + \mathrm{C3}\times\mathrm{B}^2$$

where $\mathrm{B} = \mathrm{Al(T)}/\mathrm{Al_{tot}} + \mathrm{C4}\times(1 - \mathrm{Mg(T)} - \mathrm{Al(T)}) + \mathrm{C5}\times(2 - \mathrm{Al(M)} - \mathrm{Mg(M)})$, and C1 to C5 are the fitting coefficients. The second term of the above equation takes into account the compositional influence of the cations in the tetrahedral (T) site and the third term accounts the octahedral (M) site. *Princivalle* et al. (1999) modified the above geothermometer to a simple linear equation $T(^{\circ}\mathrm{C}) = 6640\times\mathrm{B}$.

The calculated temperatures based on *Princivalle* et al.'s (1999) equation for the samples analyzed by single crystal X-ray study were found to be 920 °C and 1080 °C, respectively (Table 3). The calculated higher temperature (1080 °C) falls in the range reported by *Zhou* and *Kerrich* (1992) from the Belingwe (Zimbabwe) komatiites and that of *Rollinson* (1997) reported from Inyala chromites (Table 3). Thus, the chromite equilibrium temperatures calculated from our crystal refinement data yield temperatures close to the expected komatiite solidus temperature of around 1000 °C. However, it must be mentioned that equilibration temperature estimates using the structural refinement techniques might have been affected by

the high Cr content (~1.5 a.f.u.) in the octahedral site, where Cr^{3+} has high crystal field stabilization energy. In the studied samples, presence of high Cr in the octahedral site does not allow a 'free' partitioning of Mg, Al between octahedral and tetrahedral sites (*Lenaz* et al., 2004). Hence the structural refinement data could also reflect cooling temperatures. Nevertheless, our data show that during cooling diffusional cation exchange in chromian spinel ''freezes'' at higher temperature than Mg–Fe exchange between coexisting olivine and chromian spinel.

The determined high temperatures disagree with the *P–T* conditions of greenschist facies metamorphism deduced for the host rocks. Based on the chromite associated with komatiites from the Norseman-Wiluna Greenstone Belt (Western Australia), *Barnes* (2000) showed that chromite is hardly affected by low-grade metamorphism. *Barnes* (2000) suggested that equilibrium temperatures within the range of 750 °C to 1400 °C represent relicts of the original igneous cooling in chromites affected by the greenschist facies. In the studied Nuggihalli chromites, the unoxidized nature is manifested from the single crystal refinement data and thus we think that the calculated temperatures of 775 °C to 1080 °C correspond to the original igneous cooling stage. However, the lower equilibrium temperature of the studied samples below the expected liquidus temperatures of komatiites (1100–1400 °C, *Griffin* et al., 1994) might have resulted from the varying degrees of post-cumulus re-equilibration between olivine and chromite during cooling (*Barnes*, 1998).

Pressure estimates

Köhler and *Brey* (1990) reported an experimental study of Ca-solubility in olivine and produced the first systematic results showing a pressure dependence of Ca-partitioning between clinopyroxene and olivine. We have used *Köhler* and *Brey*'s (1990) olivine-clinopyroxene geobarometry based on Ca-partitioning and calculated pressures using the equation, $P = (-T \times \ln D_{Ca} - 11982 + 3.61 \times T)/56.2$ for $T \geq (1275.25 + 2.827 \times P)$. The calculated pressures range between 13.2 and 28.1 kbar when the temperature of crystallization is taken as 1080 °C. Our calculated pressure fall within the reported range of mantle rocks (e.g. *Princivalle* et al., 2000). Because the studied rocks are closely associated with pillow lavas, the calculated pressure, temperature and the sub-calcic nature of the clinopyroxenes indicate that cooling must have been rapid (quenched) to allow preservation of upper mantle equilibrium conditions.

Determination of fO_2

The composition and stability of chromian spinels not only depend on temperature, pressure and bulk composition, but also on oxygen fugacity. The oxygen fugacity experienced by rocks in the upper mantle can be estimated by three approaches. (i) The 'intrinsic oxygen fugacity' method described by *Sato* (1965, 1972) (ii) from Fe^{3+}/Fe^{2+} ratios of quenched silicate melts (*Fudali*, 1965; *Christie* et al., 1986) (iii) by the use of geothermobarometers (*Mattiolli* and *Wood*, 1986, 1988; *Ballhaus* et al., 1990). We have calculated oxygen fugacities by using the *Ballhaus* et al. (1990) approach. Fe^{2+} and Fe^{3+} values in spinel were derived from stoichiometry. It is assumed that chromite from chromitite did not change its $Fe^{3+}/\Sigma Fe$ and

Mg–Fe values upon cooling. We have used the estimated P–T values for the calculation and oxygen fugacities were calibrated relative to the QFM buffer. The calculated oxygen fugacity values of the Nuggihalli samples range from +0.5 to +1.6 above the QFM buffer. It cannot be proven that these oxygen fugacity values reflect the original igneous crystallization conditions. The preservation of original igneous compositions can be better understood from diffusion studies on primary magmatic mineral phases like olivine and pyroxene as documented by *Rollinson* (1997) in his study of the Inyala chromitites. However, it must be emphasized that *Ballhaus* et al.'s (1990) calibration is independent of temperature and from the evidence of rapid cooling of the studied samples, we presume that the calculated fO_2 values are rather magmatic. This suggests that the studied chromite crystallized under oxidizing conditions close to the QFM buffer.

Conclusions

The studied chromite grains from chromitites in the Nuggihalli schist belt are found to have komatiitic affinity. The wider distribution of the $Fe^{2+}/(Fe^{2+} + Mg)$ (Fig. 6) in the studied samples might be a result of Mg–Fe cation exchange during subsequent metamorphism of the area. The Nuggihalli chromitites yielded temperatures ranging from 775 to 1080 °C, pressure between 13 to 28 kbar and fO_2 values ranging from 0.5 to 1.6 above the QFM buffer. The determined equilibrium temperatures may rather present the original igneous cooling stage than a low- to medium-grade metamorphic overprint. The calculated P, T and fO_2 values are indicative of an upper mantle origin of these chromites. Some of the chromite in the Nuggihalli schist belt is enclosed by ferrian chromite, which is probably a product of later metamorphism. Chemical data showed that the cores of chromite grains were not altered during the transformation of chromian spinel to ferrian chromite at the rims.

Acknowledgements

Sincere thanks are due to Prof. *H. S. Moon* of Yonsei University, Seoul, for the electron probe microanalysis and Mysore Minerals Ltd. for all the support during the fieldwork. Comments from Dr. *S. J. Barnes* and Prof. *F. Princivalle* on an earlier version helped to improve the paper. Journal reviewers, Prof. *G. Garuti* and an anonymous reviewer are acknowledged for their constructive reviews. Editor Prof. *J. G. Raith* is thanked for his comments and efficient editorial handling. *MB* thanks Prof. *B. R. Arora*, Director, Wadia Institute of Himalayan Geology for his kind support. The paper is part of the doctoral thesis of the senior author. The Department of Science and Technology, Government of India, financially supported this research.

References

Bai WE, Zhou MF (1988) Variations in chemical compositions of chrome spinels from Hongguleleng ophiolites, Xianjing, China and their significance. Acta Mineral Sinica 8: 313–323 (in Chinese)

Bailey SW, Brindley GW, Kodama H, Martin RT (1979) Report of Clay Mineral Society Nomenclature Committee. Clays Clay Minerals 27: 238–239

Ballhaus C, Berry RF, Green DH (1990) Oxygen fugacity controls in the Earth's upper mantle. Nature 348: 437–440

Ballhaus C, Berry RF, Green DH (1991) High pressure experimental calibration of the olivine-orthopyroxene-spinel oxygen geobarometer: implications for the oxidation state of the upper mantle. Contrib Mineral Petrol 107: 27–40

Barnes SJ (1998) Chromite in komatiites. I. Magmatic controls on crystallization and composition. J Petrol 39: 1689–1720

Barnes SJ (2000) Chromite in komatiites. II. Modification during greenschist to mid-amphibolite facies metamorphism. J Petrol 41: 387–409

Barnes SJ, Roeder PL (2001) The range of spinel compositions in terrestrial mafic and ultramafic rocks. J Petrol 42: 2279–2302

Bence AE, Albee AL (1968) Empirical correction factors for the electron microanalysis of silicates and oxide. J Geol 76: 382–403

Bidyananda M (2000) Petrological and crystallochemical studies of the chromite and magnetite-bearing litho-units in the Nuggihalli Schist Belt (Karnataka): their thermodynamic parameters and geotectonic evolution. Thesis, Jadavpur University (India) (unpublished)

Bidyananda M, Mitra S (2004) Room temperature ^{57}Fe Mössbauer characteristics of chromites from the Nuggihalli schist belt, Dharwar craton, southern India. Curr Sci 86: 1293–1297

Bidyananda M, Deomurari MP, Goswami JN (2003) ^{207}Pb–^{206}Pb ages of zircon from the Nuggihalli schist belt, Dharwar craton, southern India. Curr Sci 85: 1482–1485

Bird JC, Clark AL (1976) Microprobe study of olivine chromitites of the Goodnews Bay ultramafic complex, Alaska, and the occurrence of the platinum. US Geol Surv, J Res 4: 717–725

Christie DM, Carmichael ISE, Langmuir CH (1986) Oxidation states of mid-ocean ridge basalt glasses. Earth Planet Sci Lett 79: 397–411

Della Giusta A, Ottonello G (1993) Energy and long-range disorder in simple spinels. Phys Chem Minerals 20: 228–241

Della Giusta A, Carbonin S, Ottonello G (1996) Temperature-dependent disorder in a natural Mg–Al–Fe^{2+}–Fe^{3+}-spinel. Mineral Mag 60: 603–616

Dick HJB, Bullen T (1984) Chromian spinel as petrogenetic indicator in abyssal and alpine-type peridotites and spatially associated lavas. Contrib Mineral Petrol 86: 54–76

Evans BW, Frost BR (1975) Chrome spinel in progressive metamorphism – a preliminary analysis. Geochim Cosmochim Acta 39: 959–972

Fabries J (1979) Spinel-olivine geothermometry in peridotites from ultramafic complex. Contrib Mineral Petrol 69: 329–336

Fudali RF (1965) Oxygen fugacity of basaltic and andesitic magmas. Geochim Cosmochim Acta 29: 1063–1075

Griffin WL, Ryan CG, Gurney JJ, Sobolev NV, Win TT (1994) Chromite macrocrysts in kimberlites and lamproites: geochemistry and origin. CPRM Spec Publ 1A/93: 366–377

Hill R, Roeder P (1974) The crystallization of spinel from basaltic liquid as a function of oxygen fugacity. J Geol 82: 709–729

Irvine TN (1965) Chromium spinel as a petrogenetic indicator, part I. Theory. Can J Earth Sci 2: 648–672

Irvine TN (1967) Chromian spinel as petrogenetic indicator, part II. Petrologic applications. Can J Earth Sci 4: 71–103

Jafri SH, Khan N, Ahmed SM, Saxena R (1983) Geology and geochemistry of Nuggihalli schist belt, Dharwar craton, Karnataka, India. In: *Naqvi SM, Rogers JJW* (eds) Precambrian of South India. Geol Soc India Memoir 4: 110–120

Köhler TP, Brey GP (1990) Calcium exchange between olivine and clinopyroxene calibrated as a geothermobarometer for natural peridotites from 2 to 60 kb with applications. Geochim Cosmochim Acta 54: 2375–2388

Lenaz D, Andreozzi GB, Mitra S, Bidyananda M, Princivalle F (2004) Crystal chemical and ^{57}Fe Mössbauer characteristics of chromites from the Nuggihalli schist belt (India). Mineral Petrol 80: 45–57

Liipo JP, Vuollo JI, Nykanen VM, Piirainen TA (1995) Zoned Zn-rich chromite from the Naataniemi serpentinite massif, Kuhmo Greenstone Belt, Finland. Can Mineral 33: 537–545

Mattioli GS, Wood BJ (1986) Upper mantle fugacity recorded by spinel lherzolites. Nature 322: 626–628

Mattioli GS, Wood BJ (1988) Magnetic activities across the $MgAl_2O_4$–Fe_3O_4 spinel join, with application to thermobarometric estimates of upper mantle oxygen fugacity. Contrib Mineral Petrol 98: 148–162

Melcher F, Grum W, Simon G, Thalhammer T, Stumpfl EF (1997) Petrogenesis of the ophiolitic giant chromite deposits of Kempirsai, Kazakhstan: a study of solid and fluid inclusions in chromite. J Petrol 38: 1449–1458

Mitra S (1996) Fundamentals of optical, spectroscopic and X-ray mineralogy. New Age Publishers, New Delhi, pp 336

Mitra S, Bidyananda M (2001) Crystallochemical characteristics of chlorites from the greenstone belt of south India and their geothermometric significance. Clay Sci 11: 479–501

Mitra S, Bidyananda M (2003) Evaluation of metallogenic potential of the Nuggihalli greenstone belt, South India. Compt Rend Geosci 335: 185–192

Naqvi SM, Hussain SM (1979) Geochemistry of meta-anorthosites from a greenstone belt in Karnataka, India. Can J Earth Sci 16: 1254–1264

Nell J, Wood BJ (1991) High-temperature electrical measurements and thermodynamic properties of Fe_3O_4–$FeCr_2O_4$–$MgCr_2O_4$–$FeAl_2O_4$ spinels. Am Mineral 76: 405–426

O'Neill HStC, Navrotsky A (1983) Simple spinels: crystallographic parameters, cation radii, lattice energies and cation distribution. Am Mineral 68: 181–194

O'Neill HStC, Navrotsky A (1984) Cation distributions and thermodynamic properties of binary spinel solid solutions. Am Mineral 69: 733–753

O'Neill HStC, Wall VJ (1987) The olivine-orthopyroxene-spinel oxygen geobarometer, the nickel precipitation curve, and the oxygen fugacity of the Earth's upper mantle. J Petrol 28: 1169–1191

Princivalle F, Della Giusta A, De Min A, Piccrillo EM (1999) Crystal chemistry and significance of cation ordering in Mg–Al rich spinels from high-grade hornfels (Predazzo-Monzonni, NE Italy). Mineral Mag 63: 257–262

Princivalle F, Tirone M, Comin-Chiaramonti P (2000) Clinopyroxenes from metasomatized spinel-peridotite mantle xenoliths from Nemby (Paraguay): crystal chemistry and petrological implications. Mineral Petrol 70: 25–35

Proenza J, Gervilla F, Melgarejo JC, Bodinier JL (1999) Al- and Cr-rich chromitites from the Mayarí-Baracoa ophiolitic belt (Eastern Cuba): consequence of interaction between volatile-rich melt and peridotites in suprasubduction mantle. Econ Geol 94: 547–566

Proenza J, Ortega-Gutiérrez F, Camprubí A, Tritlla J, Elías-Herrera M, Reyes-Salas M (2004) Paleozoic serpentinite-enclosed chromitites from Tehuitzingo (Acatlán Complex, southern Mexico): a petrological and mineralogical study. J South Am Earth Sci 16: 649–666

Ramakrishnan M (1981) Nuggihalli and Krishnarajpet belts. In: *Swami Nath J, Ramakrishnan M* (eds) Early Precambrian Supracrustals of Southern Karnataka. Geol Surv India Memoir 112: 61–70

Roeder PL, Campbell IH, Jamieson HE (1979) Re-evaluation of the olivine-spinel geothermometer. Contrib Mineral Petrol 68: 325–334

Rollinson H (1997) The Archean komatiite-related Inyala chromitite, Southern Zimbabwe. Econ Geol 92: 98–107

Sack RO, Ghiorso MS (1991) Chromian spinels as petrogenetic indicators: thermodynamics and petrological applications. Am Mineral 76: 827–847

Sato M (1965) Electrochemical thermometer: a possible new method of geothermometry with electroconductive minerals. Econ Geol 60: 812–818

Sato M (1972) Intrinsic oxygen fugacities of iron-bearing oxide and silicate minerals under low total pressure. Geol Soc Am Memoir 135: 289–307

Steven RT (1944) Composition of some chromites of the Western Hemisphere. Am Mineral 29: 1–34

Sudhakar KS (1980) Pillow structures in serpentinites, Tagadur, Nuggihalli schist belt, Karnataka. Ind Acad Sci Proc Earth Planet Sci 89: 117–119

Zhou MF, Kerrich R (1992) Morphology and composition of chromite in komatiites from the Belingwe greenstone belt, Zimbabwe. Can Mineral 30: 303–317

Authors' addresses: *M. Bidyananda* (corresponding author; e-mail: maibam@wihg.res.in), Wadia Institute of Himalayan Geology, Dehra Dun-248001, India; *S. Mitra*, Department of Geological Sciences, Jadavpur University, Kolkata-700032, India, e-mail: sachinathm@yahoo.com